ISSN 2070-2051, Protection of Metals and Physical Chemistry of Surfaces, 2023, Vol. 59, No. 5, pp. 1010–1027. © Pleiades Publishing, Ltd., 2023.
ISSN 2070-2051, Protection of Metals and Physical Chemistry of Surfaces, 2023. © Pleiades Publishing, Ltd., 2023.

PHYSICOCHEMICAL PROBLEMS OF MATERIALS PROTECTION

Corrosion Inhibition and Adsorption Behavior of *Musa Basjoo Siebold* Leaves Extract on Mild Steel in H_3PO_4 Solution: Experimental and Theoretical Studies

Chen Zhao[a], Bilan Lin[a, *], Xinxin Zhou[a], Jiahao Zhu[a], Tianhu Duan[a], and Yuye Xu[b, **]

[a] *School of Materials Science and Engineering, Xiamen University of Technology, Xiamen, Fujian Province, P.R. China*

[b] *College of Civil Engineering, Huaqiao University, Xiamen, Fujian Province, P.R. China*

**e-mail: linbilan@xmut.edu.cn*

***e-mail: yuyexu@hqu.edu.cn*

Received May 18, 2023; revised July 17, 2023; accepted July 24, 2023

Abstract—*Musa basjoo Siebold* leaves extract (MBSLE) was utilized as green corrosion inhibitor for mild steel in 1 M H_3PO_4 solution. The inhibition behavior was studied through electrochemical tests. The chemical structure of extract was investigated by FTIR and UV–Vis spectra. The element compositions in adsorption film on the surface of mild steel were analyzed by XPS technique. The corrosion morphology of mild steel was observed. The adsorption mechanism of typical components in extract were theoretically calculated by DFT and MD. The results showed that the inhibition efficiency of MBSLE on mild steel increased with extract concentration and MBSLE acted as a mixed corrosion inhibitor. MBSLE contained carbonyl, carboxyl, hydroxyl, heterocyclic ring, benzene ring and other polar groups, and successfully adsorbed on mild steel to form the protective film. DFT simulations proved that the active components possessed the synergistic adsorption ability to donate and receive electrons. MD calculations demonstrated the parallel adsorption of typical ingredients on steel surface, the presence of physical adsorption and the inhibition mechanism of geometric coverage effect. Irenolone in MBSLE with more aromatic rings and polar groups shows an excellent corrosion inhibition performance.

Keyword: *Musa basjoo Siebold* leaves, extract, steel, corrosion, electrochemical, chemical analysis

DOI: 10.1134/S2070205123700934

1. INTRODUCTION

Mild steel, due to excellent mechanical properties and low price, has been widely used in oil and gas pipelines, bridges, tunnels, automobiles, energy, chemicals, civil buildings and other fields [1, 2]. However, the corrosion problems usually lead to the premature failure of steel components, the huge economic losses and the unpredictable safety hazards, and corrosion control has been extensively concerned [1]. Corrosion inhibitors added to the corrosive media are one of the most effective and practical methods to retard steel corrosion [3, 4]. Unfortunately, the usable inorganic and synthetic corrosion inhibitors are expensive, difficultly biodegradable, non-renewable, toxic, and other environmental problems [5, 6]. It is urgent to develop new corrosion inhibitors which are cheap and eco-friendly. Plant extract has been qualified as one of the research directions [5, 6]. Organic substances in plant extract possess special electronic structures such as aromatic rings, heterocycles, heteroatoms, carbonyl, hydroxyl, carboxyl groups which have a great number of π electrons and (or) lone-pair electrons and are able to share electrons with metals to form chemical bonds. These active components are thus adsorbed on metal surface to slow down corrosion. Additionally, the extraction process is simple, economic and will not generate by-products; the raw sources of plants are renewable and green; and the corrosion inhibition efficiency is pleasant [4, 7, 8].

At present, researches on corrosion inhibitors of plant extracts have been carried out and achieved the gratifying results [1, 9, 10]. The inhibition behavior of *Calendula officinalis* flower heads extract on carbon steel in HCl solution was investigated by weight loss, electrochemical and microanalysis techniques, and the results showed that the extract was a mixed inhibitor with inhibition efficiency for more than 90% [1]. The water extract of *Litchi* peel was also a mixed inhibitor for carbon steel in 0.5 M H_2SO_4 solution; the inhibition efficiency increased with extract concentration (i.e. 97.8% at 3.0 g/L); and the adsorption conformed to Langmuir isotherm [9]. The inhibition efficiency of *Mango* leaves extract on carbon steel in 1 M HCl medium was 92%, showing a mixed inhibition and the Langmuir isotherm [10]. The ethanol extract of D*urian* pulps and cores also was a mixed inhibitor for

copper in 0.5 M H_2SO_4 solution, with inhibition efficiency of 92.6% at 600 mg/L; and molecular dynamics (MD) simulations showed that the main components in extract tended to adsorb on the copper surface in a parallel manner [11].

Musa basjoo Siebold is a perennial herb of *Musa* genus [12, 13]. The plant of *Musa basjoo Siebold* is high. The leaves are oblong and bright green, commonly used as the raw materials for papermaking. The fruits, flowers, leaves and roots can be used as medicine and food. The planting conditions are convenient. The water extract of the roots contains proteins, amino acids, sugars, organic acids, saponins, etc; and the alcohol extract has anthraquinone, flavonoids, coumarin, phenols, cardiac glycoside, proteins, amino acids, and so on [14]. Based on ultrasonic extraction with ethanol and enzymatic hydrolysis with cellulase and pectinase, phenols such as catechin, coumaric acid, chlorogenic acid, ferulic acid, rutin, vanillic acid were obtained from the leaves and stems of *Musa basjoo Siebold* [15]. The leaves and immature fruits of *Musa basjoo Siebold* were pretreated with kanamycin and then extracted with solvent of ethyl acetate, the bioactive phenols of irenolone was obtained [16]. 5-hydroxytryptamine, caffeic acid and L-tyrosine were founded in MBSLE [17], and lufenone and stigmasterol were also detected in their methanol extract by HPLC [18]. Therefore, MBSLE contains flavonoids, polyphenols, amino acids and other components [19]. The heteroatoms, double bonds, aromatic rings, heterocycles, hydroxyls, carbonyls, carboxyls are rich in π electrons and (or) lone pair electrons, which can share electrons with the 3*d* orbits of transition metals. The active components can be adsorbed on metal surface. MBSLE has a great potential in corrosion inhibition for metals [20].

However, literature on MBSLE as corrosion inhibitor is rare [12, 17, 20]. Chen et al., [12] obtained MBSLE by hydrothermal extraction and investigated the inhibition performance for carbon steel in HCl medium by mass loss and eletrochemical tests. MBSLE was a mixed corrosion inhibitor, and the adsorption of the extract molecules obeyed the Dhar-Flory-Huggins isotherm [12]. The *banana* peel extract also was a mixed inhibitor for X70 steel in HCl solution, with the inhibition efficiency of about 90% [17]. The adsorption conformed to the Langmuir isotherm and tended to adsorb in a parallel manner [17]. HPLC test showed that the acetone extract of *banana* peel was rich in gallic acid and catechin, and the inhibition efficiency of the raw *banana* peel extract for carbon steel in HCl solution was better than that of the mature and over mature *banana* peel [20].

H_3PO_4 is one of the important basic raw materials in industrial production, and also is one of the common chemical cleaners for production equipment. It has been mainly used in electroplating, pharmaceutical, phosphate and metallurgical industries [21]. H_3PO_4 is a medium inorganic acid and has certain corrosion effect on metals. Therefore, corrosion inhibitor is often used in H_3PO_4. The inhibition effect of various inhibitors on carbon steel in H_3PO_4 have been reported [21–24]. *Jasminum nudiflorum* extract was used as corrosion inhibitor for cold rolled steel in H_3PO_4 [23]. The results showed that the adsorption of the extract on steel complied with the Temkin isotherm, and the inhibition effect changed with the extract concentration, medium temperature, corrosion time, and H_3PO_4 concentration [23]. *Ginkgo biloba* extract was acted as a mixed inhibitor for cold rolled steel in 1 M H_3PO_4 solution according to weight loss and electrochemical measurements; the inhibition efficiency increased with extract concentration and temperature; and the adsorption followed the Langmuir isotherm [24]. However, research on inhibition and adsorption behavior of MBSLE as green corrosion inhibitor for mild steel in H_3PO_4 medium has not been explored.

In this study, organic substances extracted from *Musa basjoo Siebold* leaves were used as green and renewable corrosion inhibitor for mild steel in 1 M H_3PO_4 medium. The characteristic functional groups in extract and the interaction of active compounds and iron were investigated via FTIR and UV–Vis spectra. The compositions of the adsorption film on the surface of mild steel were analyzed by XPS. The effect of MBSLE concentration on corrosion behavior of mild steel was studied by electrochemical tests. The corrosion morphology of mild steel was observed. Frontier molecular orbital distributions, chemical reactivity, adsorption behavior of the typical components in MBSLE was calculated by density functional theory (DFT) and MD simulations. The inhibition and adsorption mechanism of the extract were clarified.

2. EXPERIMENTAL

2.1. Extraction of MBSLE

The fresh *Musa basjoo Siebold* leaves were picked from campus in Xiamen University of Technology. After washing and drying naturally, the leaves were further dried to a constant weight in an oven at 80°C. Subsequently, they were crushed and shifted through a 60-mesh sieve to remove the coarse particles. The powder of *Musa basjoo Siebold* leaves was obtained.

To achieve more active ingredients, a mixture of ethanol and distilled water with the volume ratio of 4 : 1 was selected as the extraction solvent based on the principle of similarity compatibility. An appropriate amount of the above powder was added to an extraction solvent of 400 mL and stirred thoroughly, and then ultrasonic vibrated at 40°C for 4 h to dissolve more organic substances based on the mechanical cavitation effect. The supernatant was vacuum filtered to remove the undissolved particles. The filtrate was subsequently concentrated in a rotary evaporator and

the extraction solvent was recovered. Finally, the ultra-concentrated extraction liquid was dried sufficiently in an oven at 80°C. The dark brown solid, i.e., MBSLE, was obtained.

2.2. Materials and Corrosion Medium

The tested material was mild steel, and the chemical compositions were as follows (wt %): 0.13 C, 0.38 Mn, 0.02 Si, 0.014 P, 0.031 S, and balanced Fe. The specimen size was 10 × 10 × 3 mm.

The corrosion medium was 1 M H_3PO_4 solution, diluted from 85 wt % H_3PO_4. The mass concentration of MBSLE was 0, 0.1, 0.3, 0.5, and 0.8 g/L, respectively. The medium temperature was 298, 308, and 318 K, respectively. The corrosion solution was prepared with distilled water.

2.3. Preparation of Working Electrode

Firstly, a copper conductor was welded on a large surface of 10 × 10 mm of the mild steel sample and the back was served as the working surface. Secondly, the copper wire was wrapped up three layers of heat shrinkable tubes to avoid the galvanic corrosion effect. Thirdly, excepted the working surface, all surfaces were insulated with epoxy resin. Then, the working surface was ground step by step with waterproof sandpapers ranged from nos. 400 to 2000. Finally, the polished surface was scrubbed with acetone, rinsed with distilled water and dried with cold air. The working electrode of mild steel with a working area of 1 cm^2 was obtained.

2.4. Electrochemical Measurements

The electrochemical measurements included open circuit potential (OCP), electrochemical impedance spectroscopy (EIS) and potentiodynamic polarization (PDP) curves. Two latter tests should be carried out in a relatively stable system after the OCP measurement. Therefore, OCP was monitored to judge the speed of electrochemical system reaching the dynamic equilibrium. The OCP observation time was one hour to compare the effects of MBSLE concentration on the stability of the system and to obtain a more stable OCP value.

EIS is a frequency domain technique to reveal the corrosion electrochemical information of the metal/solution interface. The frequency range was from 100 kHz to 0.01 Hz. The initial potential was the stable OCP, and the amplitude of AC signal was 10 mV. EIS testing is often considered as a non-destructive technology. The Zview software was used to fit the EIS diagram.

For PDP test, the polarization potential in a stable electrochemical system is changed with an appropriate rate and the corresponding polarization current is recorded. The PDP curves such as linear polarization, weak polarization, Tafel polarization are obtained. In this study, Tafel curves of strong polarization were measured with potential ranged from −300 to 300 mV vs. OCP. The scanning rate of 1 mV/s, which is commonly used in corrosion system, was selected. The polarization parameters were fitted with the software attached to the instrument. E_{corr} is the corrosion potential of mild steel; i_{corr} is the corrosion current density. b_c and b_a are the cathodic and anodic Tafel polarization slopes, respectively. η was the corrosion inhibition efficiency of MBSLE for mild steel, calculated by the following expression [24–26]:

$$\eta = \frac{i_{corr,0} - i_{corr,i}}{i_{corr,0}} \times 100\%, \quad (1)$$

where $i_{corr,\,0}$ and $i_{corr,\,i}$ are the corrosion current density of mild steel in 1 M H_3PO_4 solution without and with MBSLE inhibitor, respectively.

The above electrochemical tests were carried out under CS350 electrochemical workstation (Wuhan Corrtest Instruments Corp., Ltd., China). The standard three-electrode system was adopted. The working electrode was the tested mild steel electrode; the reference electrode was the saturated calomel electrode (SCE); and the auxiliary electrode was the platinum electrode. To ensure the reliability of the results, more than three parallel tests were performed for each process.

2.5. Chemical Composition Characterizations

The functional groups of the active ingredients in the plant extract directly determine the adsorption performance. MBSLE was thoroughly dried to a constant weight. The transmittance was measured by FTIR spectrometer (ALPHA; Bruker, Germany). The wavenumber was in the range from 400 to 4000 cm^{-1}. According to the peak positions, the functional groups in MBSLE were qualitatively analyzed.

The interaction between the active components and the metal atoms in the corrosive medium also has an important impact on their adsorption behavior. A 1 M H_3PO_4 solution containing 0.5 g/L MBSLE were prepared in duplicate. A polished and cleaned mild steel sample was immersed in one solution for 24 h, while the other was unchanged. The absorbance of two solutions, i.e. before and after immersion of mild steel, was measured by UV–Vis spectrophotometer (SPECORD 210/Plus; Analytik Jena, Germany). The wavelength range was from 190 to 800 nm, and the scanning interval was 1 nm. Distilled water was used as the reference solution. Combining with the shift of the position and the intensity of the spectral peaks, the interactions between active ingredients and metals can be assessed.

The polished and cleaned mild steel was corroded in 1 M H_3PO_4 solution containing 0.5 g/L MBSLE for

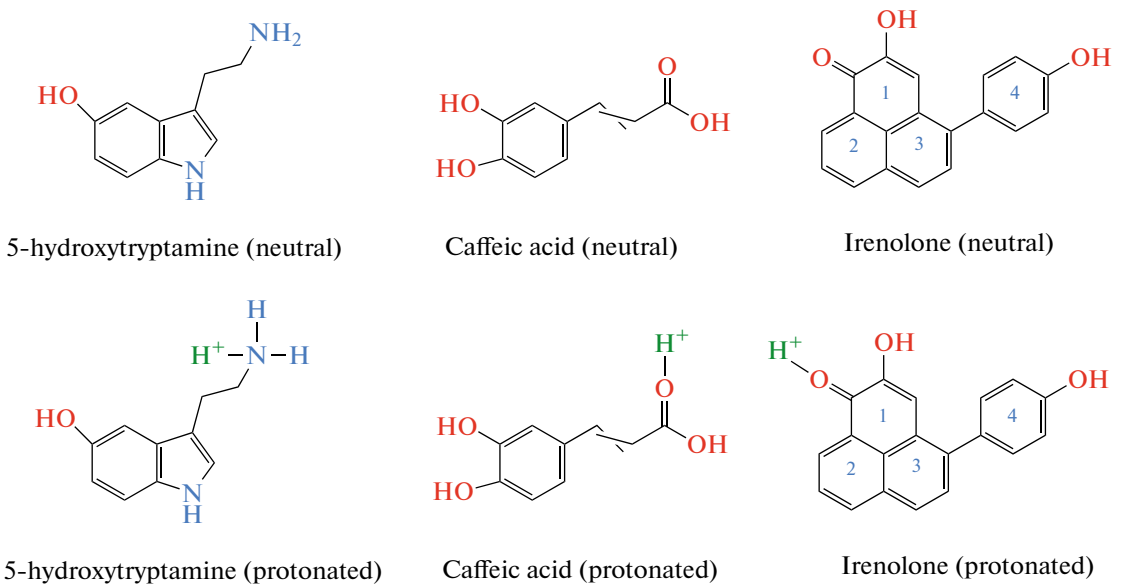

Fig. 1. Molecular structures of three typical components selected from MBSLE for theoretical calculations.

3 h, followed by rinsing with distilled water and drying with cold air. The total elements of the corrosion products (i.e., adsorption film) on the surface of mild steel were analyzed by XPS (Thermo Fisher Scientific Kα+, UK), and then the high-resolution XPS spectrum of each element was recorded. The voltage was 15 kV. The light resource was the monochromatic Al-K_α X-ray with energy of 1486.68 eV. The X-ray beam spot was 300 × 700 μm^2. All XPS spectra were corrected by the C 1s peak with binding energy of 284.8 eV. To study the existence forms of the elements in MBSLE adsorption film, the XPSPEAK41 software was used to fit the peaks of the high-resolution XPS spectrum. According to the type and existing state of elements, the adsorption of organic components in MBSLE on the surface of mild steel was determined.

2.6. Corrosion Morphology

The effect of MBLSE on the surface corrosion morphology of mild steel in 1 M H_3PO_4 solution was analyzed by SEM (EVO 18; Zeiss, Germany). The processing methods of the corroded samples were similar to that described in XPS analysis.

3. DETAILS OF THEORETICAL CALCULATIONS

3.1. Molecule Selection

To further understand the relationship of the molecular structure, adsorption performance and inhibition mechanism, DFT and MD simulations were conducted. Before theoretical calculations, the typical components should be selected from MBSLE and the molecular configurations should be constructed. Three active components of 5-hydroxytryptamine, caffeic acid and irenolone in MBSLE were chosen as the representatives of amino acids, organic acids and polyphenols, respectively. Caffeic acid also belongs to polyphenols. Figure 1 shows the corresponding molecular configurations. Three typical ingredients contain aromatic rings, hydroxyls, and (or) carbonyls, carboxyls. In addition, organic molecules in acidic medium will be protonated to form onium ions which are positively charged, as shown in Fig. 1. Obviously, the protonation of organic molecules will affect the adsorption and corrosion inhibition behaviors. The corresponding calculations for the protonated molecules were also carried out.

3.2. DFT Simulation

To evaluate the adsorption capacity of three typical molecules on the surface of mild steel, the electronic structures in the neutral and protonated forms were investigated by frontier molecular orbital theory. The quantum chemical simulation was carried out using Gaussian09 software. The geometric structures of the molecules was optimized on the basis of DFT. The 6-311** (*d*, *p*) basis set function of B3LYP was selected [10]. To more accurately simulate the adsorption of active molecules on the steel surface, the solvent effect of water was considered in this study. Combined with the Gaussian snapshots, the distributions of the highest occupied molecular orbital (HOMO) and the lowest unoccupied molecular orbital (LUMO) of three typical molecules in the neutral and protonated forms were analyzed. The global reaction activity parameters were calculated. The chemical stability of the active molecules and the ability to provide and receive elec-

trons between the 3*d* orbitals of iron atoms were assessed.

3.3. MD Simulation

To further reveal the internal relationship between the adsorption and corrosion inhibition behaviors of active components in MBSLE, the adsorption pattern and the coverage efficiency of three typical molecules on the surface of mild steel were investigated by MD simulation. The Force module in Materials Studio (MS) software was employed [27]. The Fe(110) plane, due to the lowest surface energy, i.e., the most stable surface, was selected as the adsorption surface. Six layers of iron atoms were set. The super-cell with the size of 24.7312 × 24.7312 × 40.8793 Å was constructed. The thickness of the vacuum layer was 30 Å. One selected molecule and 500 water molecules were filled. The force field of COMPASS and the ensemble of NVT were selected, and Andersen Thermostat was used to control the system temperature. The time step was 1 fs; the result was output every 5000 steps; and the total simulation time was 500 ps. To determine the existence of physical adsorption of the inhibitor molecules on the surface of mild steel, the Coulomb interaction of van der Waals bonds was also calculated using Atom-based method. Finally, the adsorption energy was also calculated to explore the adsorption capabilities of different components.

4. RESULTS AND DISCUSSION

4.1. Chemical Composition Analyses

4.1.1. FTIR spectrum of MBSLE. Figure 2 shows the FTIR spectrum of MBSLE. The first broad absorption band around 3532 cm^{-1} corresponds to the stretching vibration of hydroxyl [28]. The absorption band situated at 2929 cm^{-1} can be attributed to the stretching vibration of C–H in aromatic ring, $-CH_2$ and (or) $-CH_3$. The absorption band located at 1660 cm^{-1} is corresponding to the stretching vibration of C=O [6]. The strong and sharp absorption band seated at 1581 cm^{-1} is owing to the stretching vibration of C=C [29, 30]. The peak at 1395 cm^{-1} is related to the bending vibration of $-CH_3$ [31, 32]. The absorption peak at 1293 cm^{-1} corresponds to the bending vibration of the C–H plane. The absorption band at 1046 cm^{-1} may be due to the stretching vibration of C–C and (or) C–N [33]. The absorption band in the range from 1600 to 1000 cm^{-1} may also be the skeleton vibration region of benzene ring and (or) hetero-aromatic ring [34]. The absorption band at 995 cm^{-1} is attributed to the bending vibration of C–H [32, 33]. FTIR results indicate that there are many adsorptive functional groups such as O–H, C=O, C=C, C–N and aromatic rings in MBSLE, which are also present in three typical components of 5-hydroxytryptamine, caffeic acid and irenolone. These groups contain a great many of π electrons and (or) lone pair electrons. Meanwhile, iron atoms possess the unfilled and filled 3*d* orbits. In corrosive medium, π electrons and lone pair electrons in organic molecules may be donated to the unfilled 3*d* orbits of iron atoms. Simultaneously, lone pair electrons in extract may receive electrons from the filled 3*d* orbits of iron. The electron sharing between organic molecules and iron atoms is achieved, generating the coordination bonds. Organic molecules are thus adsorbed on the surface of steel to form the adsorption film and to protect steel from corrosion. It suggests that the active ingredients in MBSLE are qualified as the corrosion inhibitor for mild steel.

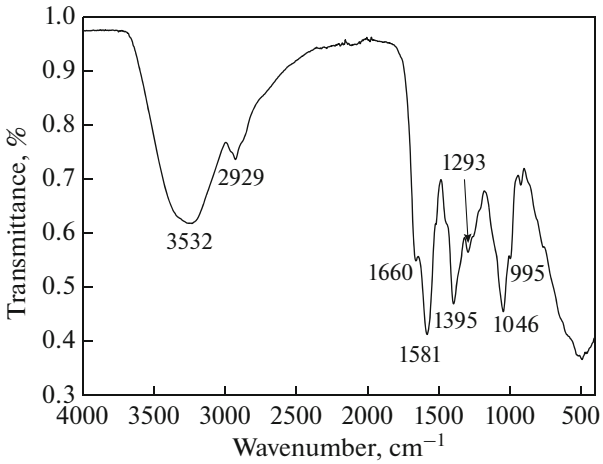

Fig. 2. FTIR spectrum of MBSLE.

4.1.2. UV–Vis spectra of corrosion solution containing MBSLE. The UV–Vis spectra of 1 M H_3PO_4 solution containing 0.5 g/L MBSLE before and after immersion of mild steel are reported in Fig. 3. Before the corrosion of mild steel, the strong peak around 195 nm and the weak peaks close to 200 and 210 nm are attributed to the π-π* transition of C=C in the aromatic rings [32, 35–37]. The broad and small absorption peak near 266 nm corresponds to the *n*-π* transition of the carbonyl group [38]. After mild steel was impregnated, the shape of the spectrum is hardly changed, but the peak intensity is decreased and the peak positions are somewhat shifted. The absorption peaks corresponding to the π-π* transition of C=C are blue-shifted slightly, which successively are 192, 197, and 208 nm. The absorption peak attributed to the n-π* transition of C=O is lightly red-shifted, about 269 nm. The shifts of the peaks, especially the red shift of C=O, indicate that the organic substances in MBSLE interact with Fe^{2+} on the surface of mild steel and form the chelates, which play an important role in inhibiting the corrosion of mild steel [39, 40].

4.1.3. XPS spectra of corrosion product film on the steel surface. When the cleaned mild steel were immersed in 1 M H_3PO_4 solution containing 0.5 g/L

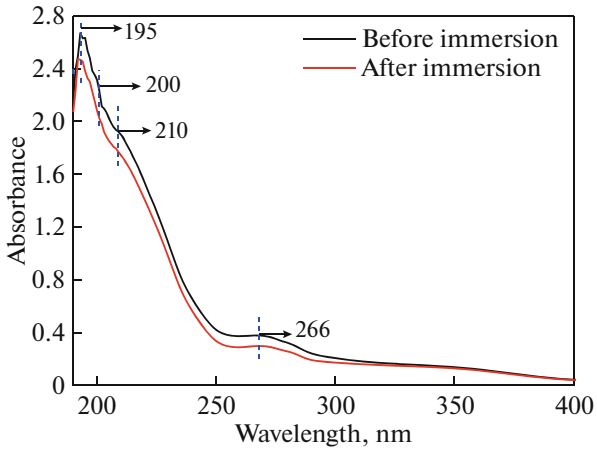

Fig. 3. UV–Vis spectra of 1 M H_3PO_4 solution containing 0.5 g/L MBSLE before and after immersion of mild steel.

MBSLE, a series of chemical reactions took place. The corrosion products, including the adsorption film of MBSLE, were formed on the surface of mild steel. As shown in XPS full spectrum in Fig. 4a, four elements of C, O, N and Fe are detected, while the P element with binding energy about 135 eV is not found [41–43]. Phosphate ions in the corrosive medium do not participate in the formation of the adsorption film. To further clarify the existence forms of four elements and the adsorption of the active ingredients, the high resolution XPS spectra of elements are reported in Fig. 4.

In Fig. 4b, the spectrum peak of O 1*s* is very wide and can be divided into four small peaks. The strong peak situated at 530.6 eV corresponds to the oxygen element in Fe_2O_3 and Fe_3O_4; the second peak at 531.9 eV is corresponding to the oxygen element in FeOOH; the relatively broad peak at 532.4 eV is due to the oxygen element in C–O and –OH; the dwarf peak at 533.3 eV can be attributed to the oxygen element in C=O and C=O^+ [41, 44, 45]. The groups of C–O, –OH, and C=O originate from the active ingredients in MBSLE. The C=O^+ group may stem from the protonated oxygen on carboxyl in caffeic acid and (or) on carbonyl in irenolone. XPS results of O 1*s* indicate that the organic substances in MBSLE are successfully adsorbed on the surface of mild steel.

In Fig. 4c, the relatively evident peak of N 1*s* can be resolved into two small peaks with binding energy of 400.5 and 401.2 eV, corresponding to the nitrogen element in C–N and C–N^+ groups, respectively [42]. These groups obviously are related to the adsorption of amino acids and (or) nitrogen-containing heterocycles in MBSLE, such as 5-hydroxytryptamine in amino acids.

As shown in Fig. 4d, the C 1*s* peak can be divided into three small peaks. The high and strong peak at 285.5 eV corresponds to the carbon element in C–C, C=C, and C–H; the wide peak at 286.2 eV is due to the carbon element in C–N, C–N^+ and C–O; and the third peak at 289.2 eV can be attributed to C=O and C=O^+ [43, 46, 47]. XPS results of C1*s* further manifest the adsorption of the neutral and protonated molecules on the surface of mild steel. This is consistent with the XPS results of O 1*s* and N 1*s*.

As shown in Fig. 4e, the broad spectrum peak of Fe $2p_{3/2}$ is composed of three small peaks. The peak with binding energy of 710.7 eV is attributed to Fe_2O_3 and Fe_3O_4, and that at 711.5 eV corresponds to FeOOH. The peak at 713.9 eV is owing to the complex of Fe [48]. It suggests the formation of the coordination chelates of organic molecules and iron atoms through the electron sharing. Electrostatic physical adsorption may also occur between the protonated molecules and the negatively charged steel surface. The former is positively charged, while the latter is due to the adsorption of phosphate ions. XPS results of Fe $2p_{3/2}$ and O 1*s* confirm the formation of the corrosion products of Fe_2O_3, Fe_3O_4, and FeOOH on the surface of mild steel.

4.2. Corrosion Morphology of Mild Steel

Figure 5 shows the SEM micrographs of the corrosion morphology of mild steel immersed in 1 M H_3PO_4 solution for 3 h. In the blank solution without MBSLE, mild steel is corroded severely, with extremely rough surface. And a great number of deep and large corrosion holes are present. When 0.5 g/L MBSLE was added into 1 M H_3PO_4 solution, the surface roughness is decreased evidently and the corrosion holes almost disappear. A visible continuous protective film on the surface of mild steel can be seen. SEM observations indicate that MBSLE has a good corrosion inhibition effect on mild steel in 1 M H_3PO_4 solution.

4.3 Electrochemical Inhibition behaviors of MBSLE

4.3.1. OCP curves. The stability of the electrochemical corrosion system can be evaluated by the change of OCP with immersion time [49]. Figure 6 shows the OCP-time curves of mild steel in 1 M H_3PO_4 solution with different concentrations of MBSLE at 298, 308, and 318 K. Whether MBSLE was added or not, OCP of mild steel at three experimental temperatures tends to be stable within one hour. However, OCP tends to stabilize more easily at lower temperature. Compared with the blank case without inhibitor, MBSLE accelerates the stabilization process. MBSLE is conducive to the dynamic equilibrium of the electrochemical system. Moreover, after adding MBSLE, the stable OCP of mild steel moves towards the positive direction, but the shift amplitude is less than 45 mV. An anodic and cathodic inhibitor can be judged if the change of corrosion potential is larger than 85 mV [50, 51]. Therefore, MBSLE acts as a

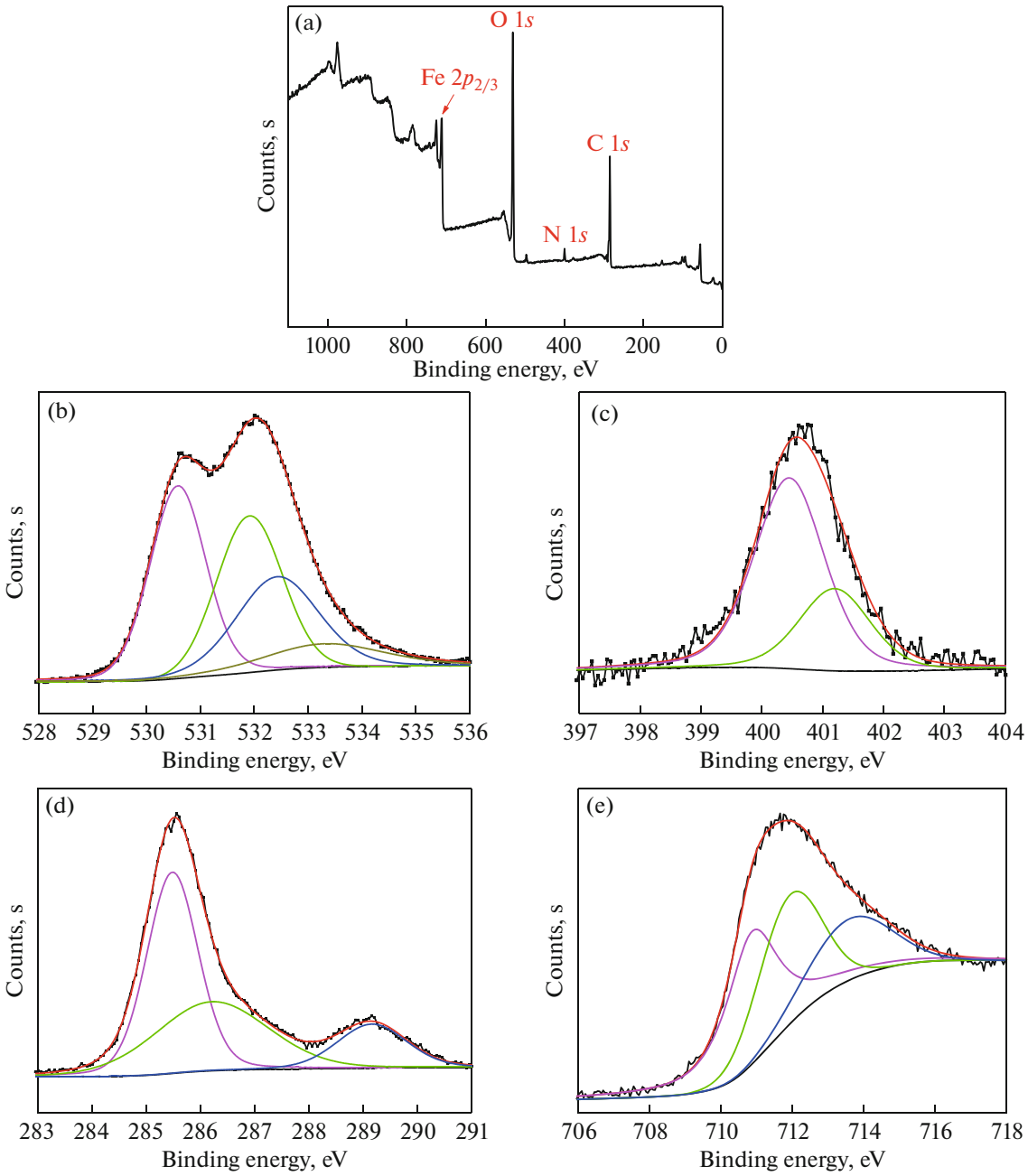

Fig. 4. XPS spectra of the corrosion product film on the surface of mild steel: (a) Survey, (b) O 1*s*, (c) N 1*s*, (d) C 1*s*, (e) Fe $2p_{3/2}$.

mixed corrosion inhibitor for mild steel in 1 M H_3PO_4 solution [50, 51].

4.3.2. PDP curves. Figure 7 shows the PDP curves of mild steel in 1 M H_3PO_4 solution containing different concentrations of MBSLE at 298, 308 and 318 K. After adding MBSLE, the anodic and cathodic polarization curves of mild steel at three experimental temperatures move to the direction where the polarization current density decreases. Both the anodic and cathodic corrosion reactions of mild steel are slowed down by MBSLE. With the increase in MBSLE concentration at fixed temperatures, the anodic and cathodic polarization currents of mild steel were first decreased obviously, then slightly increased. The continuous increase in MBSLE concentration can not continue enhancing the corrosion inhibition efficiency. This may be due to the interaction between the adsorbed molecules in MBSLE [52, 53]. The E_{corr} change at three temperatures is far less than 50 mV, further indicating that MBSLE is a mixed corrosion inhibitor.

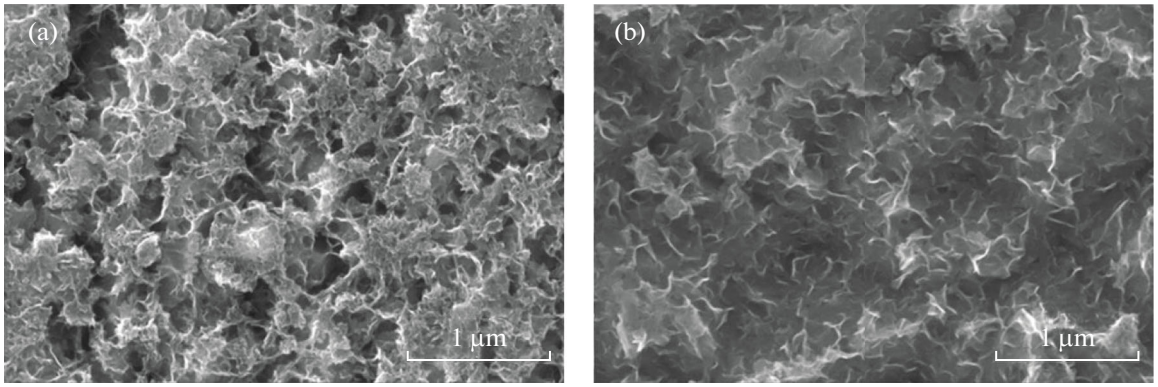

Fig. 5. Corrosion morphology of mild steel in 1 M H_3PO_4 solution: (a) without and (b) with 0.5 g/L MBSLE.

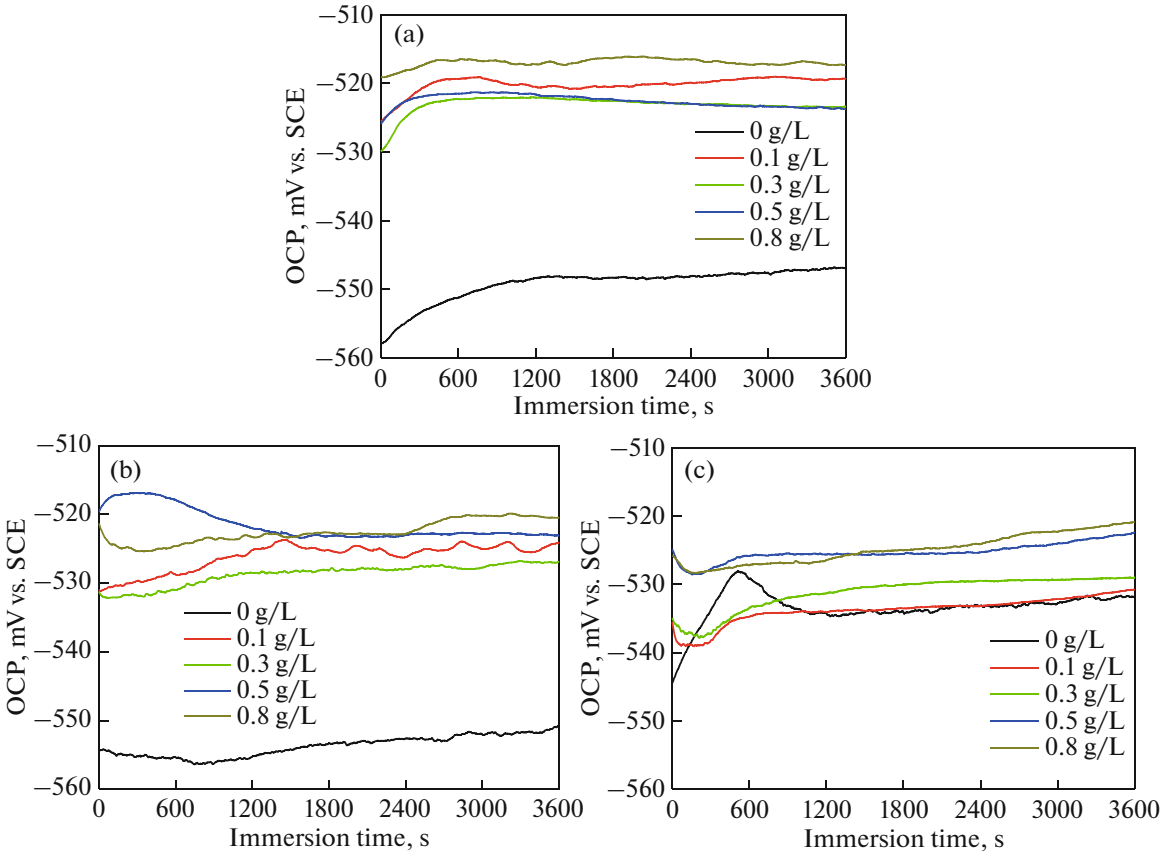

Fig. 6. OCP curves of mild steel in 1 M H_3PO_4 solution containing different concentrations of MBSLE at (a) 298, (b) 308, and (c) 318 K.

As shown in Fig. 7, the shapes of the anodic and cathodic polarization curves of mild steel are hardly changed in the absence and presence of MBSLE. The corrosion reactions of mild steel in H_3PO_4 solution are not varied. The anodic reaction is still the oxidation of iron atoms, and the cathodic reaction is the reduction of hydrogen ions. Therefore, the corrosion inhibition of MBSLE on mild steel is geometric coverage effect [54]. When some micro areas of steel surface are covered by the adsorption film of organic molecules in MBSLE, these sites and acid solution are isolated mechanically and the corrosion reactions are inhibited. On the contrary, if the micro areas are not covered by the MBSLE adsorption film, the corrosion reactions are proceeded in the original way. Therefore, the geometric coverage of the active ingredients in MBSLE directly determines the corrosion inhibition

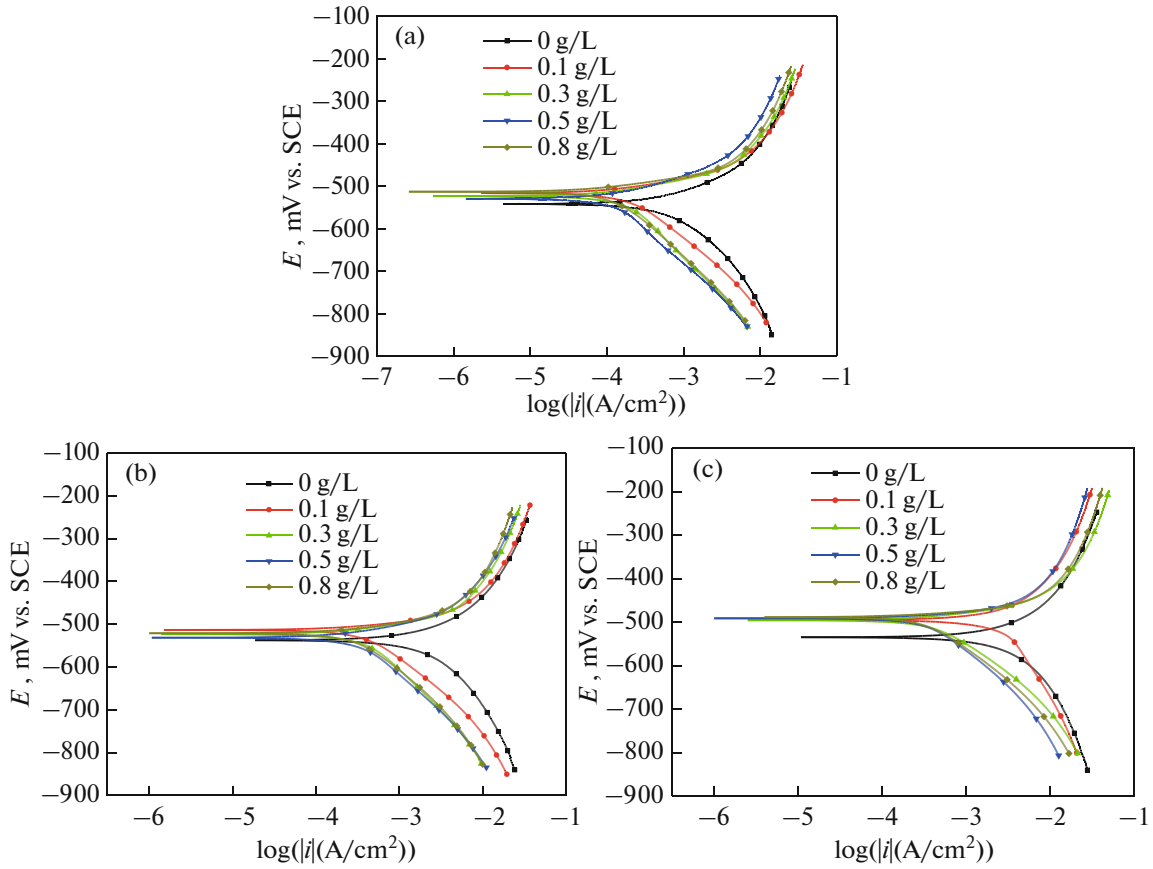

Fig. 7. PDP curves of mild steel in 1 M H_3PO_4 solution containing different concentrations of MBSLE at (a) 298, (b) 308, and (c) 318 K.

efficiency of MBSLE and the corrosion rate of mild steel. The greater the geometric coverage, the lower the corrosion rate of mild steel and the higher the corrosion inhibition efficiency of MBSLE. Increasing the coverage of the adsorption film is one of the most important factors to improve the corrosion resistance of mild steel.

Table 1 shows the polarization parameters of mild steel in 1 M H_3PO_4 solution. Due to the geometric coverage effect, the coverage (θ) of MBSLE on mild steel surface can be calculated as follows [24–26]:

$$\theta = \eta/100. \quad (2)$$

As shown in Table 1, with the increase in MBSLE concentration at three temperatures, i_{corr} of mild steel decreases first and then increases, while the change law of η and θ is just the opposite. The optimal concentration of MBSLE was 0.5 g/L at 298 and 318 K, and 0.8 g/L at 308 K. The difference may be due to the variation of adsorption mechanism such as physical adsorption, chemical adsorption and mixed adsorption [55]. The maximal η at 298, 308 and 318 K is 77.0%, 67.2 and 61.4%, respectively. i_{corr} of mild steel increases evidently with H_3PO_4 temperature, while both η and θ are decreased. The serious increase in corrosion rate of mild steel with rising temperature makes the adsorption of the active molecules on the surface of mild steel weaken. The reaction rate of hydrogen evolution controlled by the activation polarization accelerates. With the releasing of hydrogen atoms, a great mechanical peeling force is generated, hindering the adsorption of organic molecules and reducing the geometric coverage. In the previous researches on corrosion inhibitors of *Pomelo* peel extract (PPE) and *sweet potato* leaves extract (SPLE) on mild steel in H_3PO_4 and HCl media, it was found that the inhibition efficiency of both PPE and SPLE increased with medium temperature [56]. The inhibition efficiency of PPE first increased and then decreased with the extract concentration, while that of SPLE increased continuously with the extract concentration ranging from 0 to 5.0 g/L. The optimum concentration and inhibition efficiency of PPE at 318 K were respectively 3.0 g/L and 93.4%, and those of SPLE were 5.0 g/L and 96.4% [56]. Two parameters of MBSLE are apparently smaller. It can be attributed to the different active components in different extracts, resulting in the different adsorption ability and coverage. The ingredients in extracts play an important role in inhibiting corrosion.

Table 1. Effect of MBSLE concentration on polarization parameters of mild steel at different temperatures

T, K	C_{inh}, g/L	E_{corr}, mV vs. SCE	b_c, mV/dec	b_a, mV/dec	$i_{corr} \times 10^{-4}$, A/cm^2	η, %	θ
298	0	−542	−156	125	7.36	–	–
	0.1	−513	−140	123	4.27	42.0	0.420
	0.3	−524	−192	127	3.51	52.3	0.523
	0.5	−530	−170	96	1.69	77.0	0.770
	0.8	−515	−158	143	3.57	51.5	0.515
308	0	−538	−195	169	21.4	–	–
	0.1	−517	−149	163	10.3	51.9	0.519
	0.3	−525	−186	187	9.20	57.0	0.570
	0.5	−533	−170	152	7.93	62.9	0.629
	0.8	−524	−176	166	7.02	67.2	0.672
318	0	−535	−209	186	30.10	–	–
	0.1	−495	−297	204	27.91	7.3	0.073
	0.3	−499	−137	155	12.70	57.8	0.578
	0.5	−496	−154	198	11.60	61.4	0.614
	0.8	−493	−142	193	14.51	51.8	0.518

4.3.3. EIS diagrams. Figure 8 shows the Nyquist impedance diagrams of mild steel in 1 M H_3PO_4 solution containing different concentrations of MBSLE at 298 and 308 K. All Nyqusit diagrams are composed of a deformed capacitance loop at high frequency and an inductance loop at low frequency. The deformation of the capacitance loop is due to the dispersion effect caused by the uneven and rough surface of the mild steel electrode [57–59]. The capacitance arc corresponds to the electric double-layer capacitor of the interface between mild steel and corrosion solution. The inductance arc is related to both the dissolution of micro sites on the mild steel surface and the desorption and adsorption of the active components in these micro areas [60]. When the active molecules at some micro zones of mild steel are desorbed, these sites are exposed and corroded. At the same time, some organic molecules in corrosion medium migrate to these uncovered domains and then adsorb, repairing these desorbed and corroded micro regions and inhibiting the corrosion process. The larger the inductance arc, the better the repair effect of the desorption zones and the corrosion resistance of mild steel. As shown in Fig. 8, in the blank solution without MBSLE, the size of the inductance arc is very small or even disappears. This is due to the absence of the active molecules used to adsorb and repair. On the contrary, when MBSLE was added into 1 M H_3PO_4 solution, the size of the inductance arc increases.

Similar to the inductance arc, the size of the capacitance arc increases after adding MBSLE. The charge transfer resistance of corrosion reactions on the surface of mild steel enhances. With the increase in MBSLE concentration, the size of the capacitance arc first increases and then decreases. MBSLE almost does not change the shape of the Nyquist diagrams. The corrosion mechanism of mild steel in 1 M H_3PO_4 solution is not changed by MBSLE [61]. It again suggests the inhibition behavior of geometric coverage effect of MBSLE, consistent with the PDP results.

Figure 9 shows the equivalent circuit used to fit the impedance data in Fig. 8, and Table 2 lists the corresponding fitted results. Where R_s is the solution resistance. R_{ct} is the charge transfer resistance of the metal/solution interface. L is the inductance. R_L is the inductance resistance. CPE_{dl} is the constant phase element which is used to characterize the electric double-layer capacitor between the metal/solution interface and can be expressed as follows [62, 63]:

$$Z_{CPE_{dl}} = \frac{1}{Y_{0\text{-}dl}(j\omega)^{n_{dl}}}, \quad (3)$$

where $Y_{0\text{-}dl}$ is the capacitance parameter of CPE_{dl}. ω is the angular frequency, i.e., $\omega = 2\pi f$. j is the imaginary root, i.e., $j^2 = -1$. n_{dl} characterizes the deformed degree of CPE_{dl}, ranging from 0 to 1. If n_{dl} is closer to 1, the electric double-layer capacitor is closer to the flat plate capacitor. The electric double-layer capacitor (C_{dl}) can be calculated by the following expression [64–66]:

$$C_{dl} = Y_{0\text{-}dl}(2\pi f_{max})^{n_{dl}-1}, \quad (4)$$

where f_{max} is the characteristic frequency corresponding to the maximum imaginary part. Based on the EIS results, η of MBSLE can be calculated as follows [49, 67]:

$$\eta = \frac{R_{ct}^{inh} - R_{ct}^{0}}{R_{ct}^{inh}} \times 100\%, \quad (5)$$

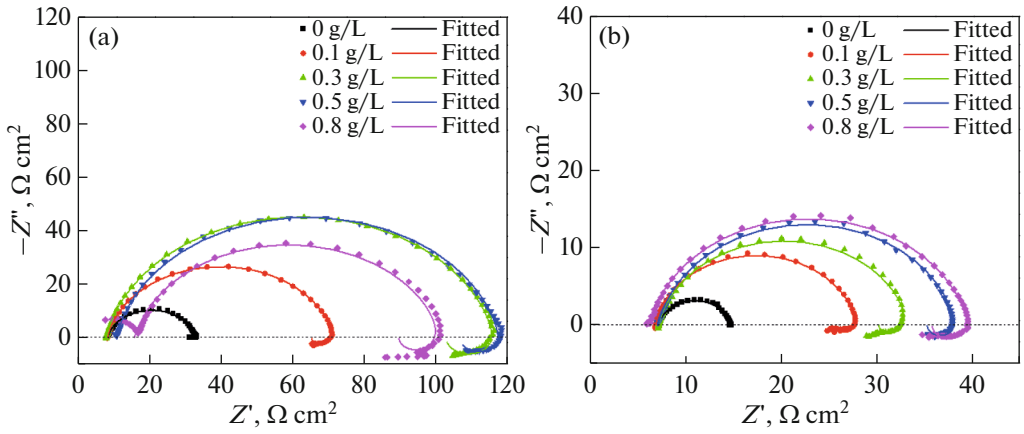

Fig. 8. Nyquist diagrams of mild steel in 1 M H_3PO_4 containing different concentrations of MBSLE at (a) 298 and (b) 308 K.

where R_{ct}^0 and R_{ct}^{inh} are the charge transfer resistance of mild steel in 1 M H_3PO_4 solution without and with MBSLE, respectively. The coverage of the active molecules on the surface of mild steel based on EIS was also calculated according to Formula (2).

As shown in Table 2, the addition of MBSLE overall has little effect on R_s of 1 M H_3PO_4 solution, but R_s is reduced with the increase in solution temperature. Increasing MBSLE concentration at fixed temperature, the R_{ct}, η and θ first increase rapidly and then decrease slightly. The increase in R_{ct} can be attributed to the protective film including corrosion products and adsorption film on the surface of mild steel, confirmed by the XPS and SEM results. The coverage of the active molecules on the mild steel surface increases with MBSLE concentration, hindering the charge transfer between the metal/solution interface and improving the corrosion inhibition efficiency. However, the values of Y_0 and C_{dl} decrease first and then increase. The prospective reasons are as follows [57, 68, 69]: 1) The active molecules in MBSLE replace the water molecules which were pre-adsorbed on the surface of mild steel, reducing the dielectric constant of the electric double-layer capacitor. 2) The adsorption of the active components in MBSLE reduces the surface roughness of mild steel, resulting in an enhancement in the smoothness and uniformity and a reduction in the true surface area of the electric double-layer capacitor. 3) The adsorption film is conducive to enlargement the distance of two electrode plates of the electric double-layer capacitor. According to the Helmholtz equation, Y_0 and C_{dl} of mild steel are thus reduced.

As shown in Table 2, n_{dl} in all cases is in the range from 0.87 to 0.91, of which the difference is extremely slight. n_{dl} also is close to 1, indicating that the electric double-layer capacitor of the steel/solution interface is similar to the ideal capacitor. n_{dl} is hardly changed by MBSLE, further reflecting the inhibition mechanism of geometric coverage effect [49, 70]. In addition, R_L and L are absent when MBSLE was absent, but they are obviously improved when MBSLE was added. With the increase in solution temperature, R_L and L decrease, and so is the inhibition efficiency. Therefore, the low-frequency inductance loop can also directly check the inhibition and repair abilities of the corrosion inhibitor in this corrosion system.

4.4. DFT Simulation

DFT simulation is profit to understand the characteristics of electronic donors and (or) receptors of organic molecules, facilitating the investigation of the interaction between inhibitor molecules and metal matrix. The volume of the frontier molecular orbital distribution directly affects the strength of the chemical reactions, the adsorption ability and the corrosion inhibition efficiency of the organic molecules. The wider the distribution and the larger the volume of HOMO of the active molecules, the more favorable it is to provide electrons to the lowest empty orbitals of metal atoms. Similarly, the wider the distribution and the larger the volume of LUMO, the more beneficial it is to accept free electrons from the outer filled orbitals of metal atoms. The above two cases will produce the stronger interaction and adsorption stability [31, 71].

Figure 10 shows the HOMO and LUMO distributions of three typical components in MBSLE at neutral and protonated states. The HOMO of neutral

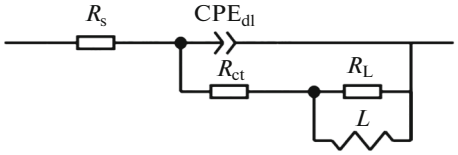

Fig. 9. Equivalent circuit used to fit the EIS diagrams in Fig. 8.

Table 2. EIS fitted parameters of mild steel in 1 M H_3PO_4 solution at different temperatures

T, K	C_{inh}, g L^{-1}	R_s, Ω cm^2	$Y_{0\text{-dl}}$, $\mu\Omega^{-1}$ cm^{-2} s^{-n}	n_{dl}	R_{ct}, Ω cm^2	R_L, Ω cm^2	L, H cm^2	C_{dl}, μF/cm^2	η, %	θ
298	0	9	118	0.89	24.2	—	—	58	—	—
	0.3	8	91	0.89	94.5	13	31	51	74.4	0.744
	0.5	11	83	0.89	95.4	11	48	48	74.6	0.746
	0.8	16	167	0.87	73.5	12	7	86	67.1	0.671
308	0	7	268	0.88	7.5	—	—	117	—	—
	0.3	7	267	0.88	23.0	3	1	138	67.4	0.674
	0.5	7	109	0.89	28.1	3	3	53	73.3	0.733
	0.8	6	105	0.88	29.6	4	5	48	74.7	0.747

5-hydroxytryptamine is mainly distributed on two aromatic rings (i.e., benzene ring, nitrogen-containing heterocycle) and the adjacent hydroxyl and methylene. These sites are rich in π electrons and lone pair electrons which can be provided to the 3*d* empty orbitals of iron atoms. The characteristic of electron donors is exhibited. Similarly, its LUMO is centered at two aromatic rings and hydroxyl. The lone pair electrons in these sites can accept the free electrons from the filled 3*d* orbitals of iron atoms. The characteristic of electron receptors is displayed. During the interaction of neutral 5-hydroxytryptamine and iron atoms, benzene ring, heterocycle and hydroxyl can act as both the electron donors and the electron acceptors. The coordination bonds and the corresponding chelates are formed through this synergistic mechanism of electron sharing. Therefore, neutral 5-hydroxytryptamine molecules are adsorbed on the surface of mild steel. During the simulation of the geometric equilibrium configuration of 5-hydroxytryptamine, the most suitable atom to be protonated is nitrogen in amino, as shown in Fig. 1. Figure 10 also manifests that the distributions of HOMO and LUMO of 5-hydroxytryptamine after protonation are almost unchanged. The protonated 5-hydroxytryptamine also demonstrates an excellent synergistic adsorption effect similar to the neutral state. Moreover, the positively charged nitrogen atom can generate the electrostatic attraction with the iron surface which is negatively charged due to the pre-adsoprtion of phosphate anions. The physical adsorption effect thus occurs. It can be inferred that 5-hydroxytryptamine in acid solution can be adsorbed on the surface of mild steel by multiple synergistic factors, forming the protective adsorption film and inhibiting the corrosion of mild steel.

As shown in Fig. 10, the HOMO distributions of caffeic acid in both neutral and protonated forms are covered on the whole molecule, i.e., one benzene ring, two hydroxyls, one C=C bond in main chain and one carboxyl. Their LUMOs at both states are also almost distributed on the whole molecule, except for one hydroxyl. Moreover, apart from a slight smaller HOMO in benzene ring 2 and LUMO in benzene ring 4, HOMO and LUMO of neutral irenolone also nearly cover the whole molecule. After protonation, both HOMO and LUMO distributions of irenolone are enlarged. Therefore, similar to 5-hydroxytryptamine, caffeic acid and irenolone in MBSLE can also be adsorbed on mild steel surface through multiple factors including chemisorption by forming coordination bonds and physical adsorption by electrostatic attraction. Three typical components of 5-hydroxytryptamine, caffeic acid and irenolone in MBSLE have good adsorption ability, confirming the XPS and SEM results.

To more accurately grasp the adsorption capacity of the inhibitor molecules on the surface of mild steel, the reaction activity parameters were calculated based on the electron wave function. The related expressions are as follows [58, 72]:

$$\Delta E = E_{LUMO} - E_{HOMO}, \quad (6)$$

$$I = -E_{HOMO}, \quad (7)$$

$$A = -E_{LUMO}, \quad (8)$$

$$\chi = \frac{I + A}{2}, \quad (9)$$

$$\varphi = \frac{I - A}{2}, \quad (10)$$

$$\Delta N = \frac{\chi_{Fe} - \chi_{inh}}{2(\varphi_{Fe} + \varphi_{inh})}, \quad (11)$$

where E_{HOMO} and E_{LUMO} are the electron energy of HOMO and LUMO, respectively. ΔE is the energy gap between LUMO and HOMO; I and A are the ionization potential energy and the electron affinity energy, respectively. χ and φ are the electronegativity and the global hardness, respectively. The subscripts of "Fe" and "inh" represent the relevant parameters for iron and inhibitor, respectively. In this paper, χ_{Fe} is 7 eV and φ_{Fe} is 0 eV [31, 71]. The higher the E_{HOMO} of

Compounds	HOMO	LUMO
5-hydroxytryptamine (neutral)	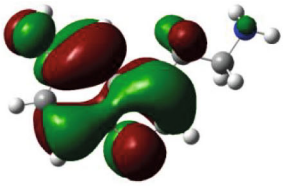	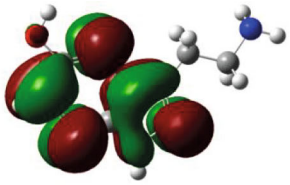
5-hydroxytryptamine (protonated)	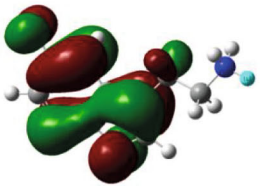	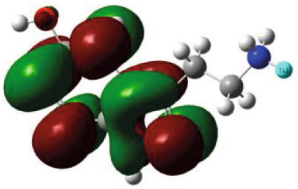
Caffeic acid (neutral)	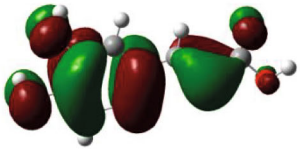	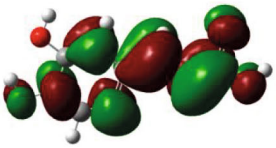
Caffeic acid (protonated)		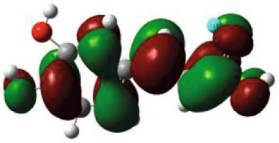
Irenolone (neutral)	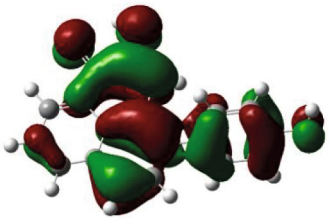	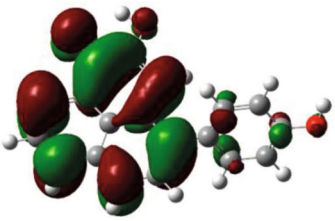
Irenolone (protonated)	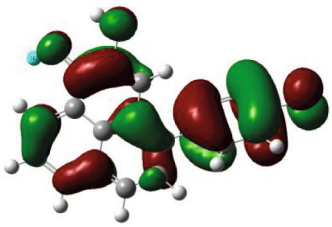	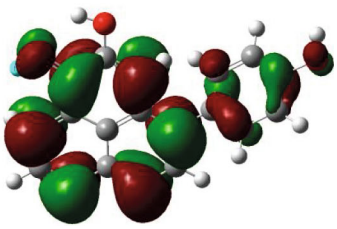

Fig. 10. HOMO and LUMO distributions of three typical components in MBSLE at neutral and protonated states.

organic molecules, the easier it is to provide electrons to metal atoms. On the contrary, the lower the E_{LUMO}, the easier it is to obtain valence electrons from metal atoms [73, 74]. Obviously, the smaller the ΔE, the poorer the molecule stability, the higher the chemical reaction activity, and the easier it is to share electrons with metal atoms and to adsorb on the metal surface [5, 25]. ΔN reflects the electron transfer ability of the active molecules. For ΔN less than 3.6, the electron donating ability of organic molecules increases with ΔN [75]. Conversely, the electron accepting ability increases with the decrease in ΔN [6, 76].

Table 3 shows the reaction activity parameters of three typical components of 5-hydroxytryptamine, caffeic acid and irenolone in MBSLE. E_{HOMO} of three typical ingredients is similar as a whole, suggesting an alike capacity to supply electrons. However, E_{LUMO} and ΔE are significantly different, decreasing in the

Table 3. Reaction activity parameters of three typical components in MBSLE based on DFT calculation

Molecules	E_{HOMO}, eV	E_{LUMO}, eV	ΔE, eV	I, eV	A, eV	χ, eV	φ, eV	ΔN, eV
Neutral state								
5-hydroxytryptamine	–5.55	–0.59	4.96	5.55	0.59	3.07	2.48	0.79
Caffeic acid	–6.02	–2.01	4.01	6.02	2.01	4.02	2.00	0.74
Irenolone	–5.90	–2.91	2.99	5.90	2.91	4.41	1.50	0.87
Protonated state								
5-hydroxytryptamine	–5.69	–0.74	4.95	5.69	0.74	3.22	2.48	0.76
Caffeic acid	–6.62	–3.44	3.18	6.62	3.44	5.03	1.59	0.62
Irenolone	–6.55	–4.05	2.49	6.55	4.05	5.30	1.25	0.68

order of 5-hydroxytryptamine > caffeic acid > irenolone. ΔE of irenolone is less than 3 eV. Irenolone has the strongest ability to share electrons with iron atoms, and so is the chemical reaction activity. The smallest φ of irenolone indicates that the reaction products with the soft iron ions in acid solution are the most stable [75]. Moreover, all ΔN is positive. ΔN of irenolone is a little greater, but the difference of ΔN for three typical components is small, further indicating a similar ability to provide electrons to iron atoms.

By carefully comparing the data in Table 3, the rules for the relative size of various activity parameters of three typical components under protonation and neutral states are similar. However, the chemical stability of three components after protonation is further reduced, and the interaction with iron atoms is enhanced. The electron donating ability after protonation is decreased, but the electron accepting ability is enhanced. DFT analysis shows that at both neutral and protonated states, the interaction of irenolone with iron atoms is the strongest, followed by caffeic acid and 5-hydroxytryptamine. Irenolone can provide the strongest corrosion inhibition effect for mild steel. This can be attributed to the different type and number of functional groups participated in electron donation and reception. Irenolone has four benzene rings, two hydroxyls and one carbonyl; caffeic acid has one benzene ring, two hydroxyls, one C=C bond and one carboxyl; and 5-hydroxytryptamine has two aromatic rings and one hydroxyl. Besides aromatic rings and C=C bond, carbonyls and hydroxyls with strong polarity also have an important contributions to the reaction activity of organic molecules with metal atoms. The reaction activity, adsorption ability and corrosion inhibition efficiency are enhanced with the increase in number of the above groups.

Table 4. E_{ads} of three typical components in MBSLE, kcal/mol

Compounds	Neutral state	Protonated state
5-hydroxytryptamine	–136.2	–294.5
Caffeic acid	–142.8	–279.5
Irenolone	–208.1	–348.8

4.5. MD Simulation

The equilibrium geometry of three typical components of 5-hydroxytryptamine, caffeic acid and irenolone on the Fe (110) plane was investigated through MD simulation, and the adsorption energy was calculated by the following expression [27, 58, 77]:

$$E_{ads} = E_{tot} - \left(E_{met+sol} + E_{inh}\right), \quad (12)$$

where E_{ads} is the adsorption energy of the inhibitor molecules on the surface of mild steel; E_{tot} is the total energy of the whole system including steel, solution and inhibitor; $E_{met+sol}$ is the total energy of the system with steel and solution; E_{inh} is the energy of the inhibitor molecules.

Figure 11 shows the final snapshots of side view and top view of three typical components of 5-hydroxytryptamine, caffeic acid and irenolone on the Fe(110) plane based on MD simulation. Table 4 presents the corresponding adsorption energy.

As shown in Fig. 11, three typical organic components at both neutral and protonated states are basically adsorbed on the Fe(110) surface in a parallel molecular conformation, facilitating the maximal coverage of the steel surface. According to the above electrochemical inhibition mechanism of geometric coverage effect, it is beneficial to optimize the corrosion inhibition efficiency. The coverage of irenolone is the largest, and that of 5-hydroxytryptamine and caffeic acid is basically similar. It also can be confirmed by the most negative E_{ads} of irenolone and the close E_{ads} of 5-hydroxytryptamine and caffeic acid at the same state. The extremely negative E_{ads} of three typical components at both states indicates a strong spontaneous adsorption tendency on the surface of mild steel. And the spontaneity is enhanced after protonation, consistent with the DFT results.

However, there are some differences between DFT and MD simulations. The HOMOs and LUMOs show

Compounds	Side view	Vertical view
5-hydroxytryptamine (neutral)	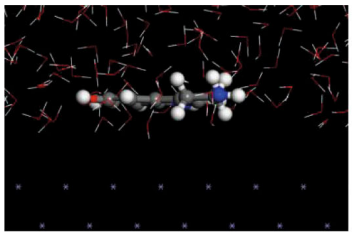	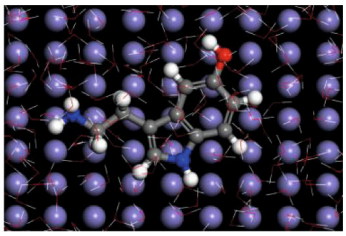
5-hydroxytryptamine (protonated)	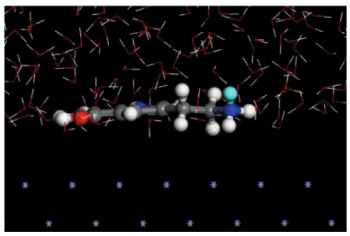	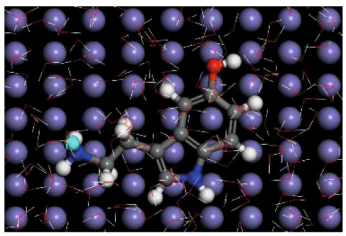
Caffeic acid (neutral)	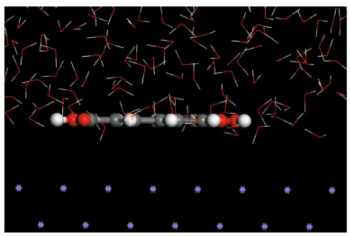	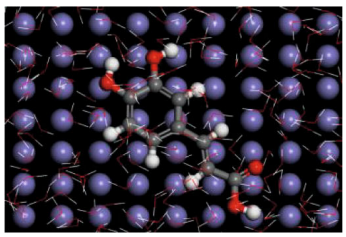
Caffeic acid (protonated)	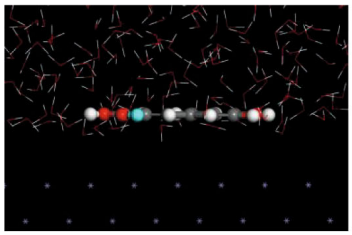	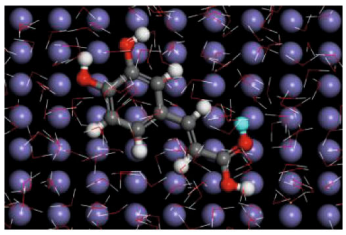
Irenolone (neutral)	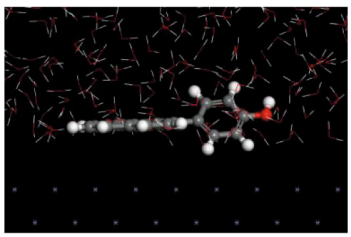	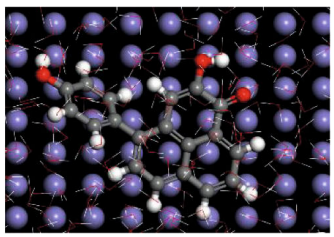
Irenolone (protonated)	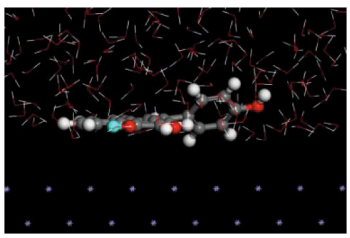	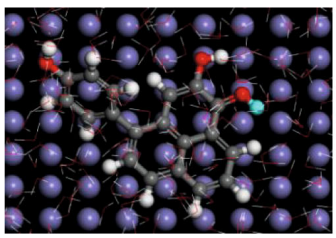

Fig. 11. Final snapshots of three neutral and protonated components in MBSLE on the surface of Fe(110) based on MD simulation.

that some groups in three typical components do not participate in sharing electrons or forming coordination bonds, as shown in Fig. 10. The final snapshots show that all atoms, except some hydrogen atoms, are adsorbed on iron atoms in a parallel manner. It indicates that there are chemical bonds and physical bonds between organic atoms and iron atoms. Obviously, chemical bonds are due to the electron sharing and generate the chemisorption, while the physical adsorption can be attributed to other factors such as electrostatic attraction, van der Waals force and so on. These different results of DFT and MD simulations suggest that the adsorption of active ingredients in MBSLE on the surface of mild steel are the mixed adsorption including chemical adsorption and physical adsorption.

5. CONCLUSIONS

The inhibition and adsorption behaviors of *Musa basjoo Siebold* leaves extract (MBSLE) as renewable corrosion inhibitor for mild steel in 1 M H_3PO_4 solution were investigated by experiments and calculations. FTIR results showed that MBSLE contain hydroxyls, carbonyls, carboxyls, heterocycles, benzene rings and other functional groups. UV–Vis results showed the interaction of some functional groups with iron in corrosive medium. XPS analysis confirmed that the functional groups in MBSLE are successfully adsorbed on the surface of mild steel to form the protective adsorption film. SEM observations proved that MBSLE effectively controls the corrosion of mild steel in H_3PO_4. The electrochemical tests showed that the corrosion inhibition efficiency of MBSLE is related to the extract concentration and the solution temperature. MBSLE acts as a mixed corrosion inhibitor. The inhibition mechanism of MBSLE is geometric coverage effect.

5-Hydroxytryptamine, caffeic acid and irenolone in MBSLE were selected as the representative components for DFT and MD simulations. The HOMOs and LUMOs suggested that the active ingredients at both neutral and protonated states display the features of electron acceptors and electron donors. The active molecules can share electrons with iron atoms through a cooperative mechanism, proving the existence of chemical adsorption. MD simulation attested the parallel and spontaneous adsorption of the organic molecules on the Fe (110) surface and the presence of physical adsorption. The adsorption of MBSLE components follows the mixed adsorption. The type and number of aromatic rings and polar groups have a great influence on reaction activity, adsorption ability and geometric coverage. Irenolone in three typical ingredients shows the most excellent corrosion inhibition efficiency.

FUNDING

This work was supported by the Natural Science Foundation of Fujian Province (nos. 2020J01291 and 2020J01059), the National Natural Science Foundation of China (no. 52178484), and the "Scientific Research Climbing Plan" of Xiamen University of Technology (no. XPD-KT20002).

CONFLICT OF INTEREST

The authors of this work declare that they have no conflicts of interest.

DATA AVAILABILITY

Data will be made available on request.

REFERENCES

1. El-Hashemy, M.A. and Sallam, A., *J. Mater. Res. Technol.,* 2020, vol. 9, no. 6, p. 13509. https://doi.org/10.1016/j.jmrt.2020.09.078
2. Hoai, N.T., Hien, P.V., Vu, N.S.H., Son, D.L., Man, T.V., Tri, M.D., and Nam, N.D., *Chem. Pap.,* 2019, vol. 73, p. 909. https://doi.org/10.1007/s11696-018-0649-6
3. Pal, A. and Das, C., *Chem. Pap.,* 2023, vol. 77, p. 1107. https://doi.org/10.1007/s11696-022-02549-7
4. Ugi, B.U. and Obeten, M.E., *Int. J. Appl. Chem.,* 2019, vol. 5, no. 2, p. 22. https://doi.org/10.14445/23939133/IJAC-V5I2P105
5. Chauhan, D.S., Quraishi, M.A., Srivastava, V., Haque, J., and El-ibrahimi, B., *J. Mol. Struct.,* 2021, vol. 1226, p. 129259. https://doi.org/10.1016/j.molstruc.2020.129259
6. Thomas, A., Prajila, M., Shainy, K.M., and Joseph, A., *J. Mol. Liq.,* 2020, vol. 312, p. 113369. https://doi.org/10.1016/j.molliq.2020.113369
7. Dehghani, A., Bahlakeh, G., Ramezanzadeh, B., and Ramezanzadeh, M., *J. Mol. Liq.,* 2020, vol. 310, p. 113221. https://doi.org/10.1016/j.molliq.2020.113221
8. Mourya, P., Banerjee, S., and Singh, M.M., *Corros. Sci.,* 2014, vol. 85, p. 352. https://doi.org/10.1016/j.corsci.2014.04.036
9. Singh, M.R., Gupta, P., and Gupta, K., *Arabian J. Chem.,* 2015, vol. 52, no. 7, p. 1035. https://doi.org/10.1016/j.arabjc.2015.01.002
10. Ramezanzadeh, M., Bahlakeh, G., Sanaei, Z., and Ramezanzadeh, B., *Appl. Surf. Sci.,* 2019, vol. 463, no. 1, p. 1058. https://doi.org/10.1016/j.apsusc.2018.09.029
11. Hu, Y.Z., Fan, B.M., Liu, H., Fan, G.F., Hao, H., and Yang, B., *Corros. Prot.,* 2020, vol. 41, no. 7, p. 17. https://doi.org/10.11973/fsyfh-202007003
12. Chen, W., Tao, Y.Y., Guan, C.P., and Hu, X.A., *Surf. Technol.,* 2016, vol. 45, no. 1, p. 124. https://doi.org/10.16490/j.cnki.issn.1001-3660.2016.01.020

13. Liu, Y., Lu, Q., Zhou, Z.Y., and Chen, J.C., *J. Guangdong Pharm. Univ.,* 2013, vol. 29, no. 6, p. 675. https://doi.org/10.3969/j.issn.1006-8783.2013.06.024
14. Sun, Y.C., Wang, X.P., Jin, F.Y., Huang, J., and Wei, F., *Lishizhen Med. Mater. Med. Res.,* 2009, vol. 20, no. 2, p. 360. https://doi.org/10.3969/j.issn.1008-0805.2009.02.054
15. Feng, Y., Lan, P., Li, K.C., Lan, L.H., Li, M., Lu, Y.Y., Liao, Y.X., Lan, X.D., Xie, T., Wei, D.P., Tan, Q., and Meng, Y.L., CN Patent CN112353881A, 2021.
16. Luis, J.G., Echeverri, F., Quinones, W., Brito, I., López, M., Torres, F., Cardoan, G., Aguiar, Z., Pelaez, C., and Rojas, M., *J. Org. Chem.,* 1993, vol. 58, no. 16, p. 4306. https://doi.org/10.1021/jo00068a027
17. Guo, L., Tan, B., Li, W.P., Li, Q.B., Zheng, X.W., and Obot, I.B., *J. Mol. Liq.,* 2020, vol. 327, p. 114828. https://doi.org/10.1016/j.molliq.2020.114828
18. Wu, H.M., Kong, J., Huang, X.L., Yang, X.S., and Wang, X.P., *China Pharm.,* 2021, vol. 32, no. 5, p. 542. https://doi.org/10.6039/j.issn.1001-0408.2021.05.06
19. Li, G.C., Chen, R., Zhang, R., and Tang, Y.J., *J. Hunan Inst. Eng. (Nat. Sci. Ed.),* 2015, vol. 25, no. 3, p. 59. https://doi.org/10.15987/j.cnki.hgbjbz.2015.03.015.
20. Ji, G., Anjum, S., Sundaram, S., and Prakash, R., *Corros. Sci.,* 2015, vol. 90, no. 1, p. 107. https://doi.org/10.1016/j.corsci.2014.10.002
21. Huang, K.Y., *Clean. World,* 1998, vol. 1, p. 30. https://doi.org/CNKI:SUN:HXQX.0.1998-01-008.
22. Deng, S.R., Li, X.H., and Fu, H., *Total Corros. Control,* 2011, vol. 25, no. 11, p. 42. https://doi.org/10.13726/j.cnki.11-2706/tq.2011.11.011
23. Yi, Y.L., Chen, Y.Q., Tao, Y., Yu, M., and Li, X.H., *Clean. World,* 2016, vol. 32, no. 9, p. 30. https://doi.org/CNKI:SUN:HXQX.0.2016-09-008.
24. Berrissoul, A., Ouarhach, A., Benhiba, F., Romane, A., Guenbour, A., Outada, H., and Dafali, A., *J. Mol. Liq.,* 2021, vol. 349, p. 118102. https://doi.org/10.1016/j.molliq.2021.118102
25. Berrissoul, A., Ouarhach, A., Benhiba, F., Romane, A., Zarrouk, A., Guenbour, A., Dikici, B., and Dafali, A., *J. Mol. Liq.,* 2020, vol. 313, p. 113493. https://doi.org/10.1016/j.molliq.2020.113493
26. Wang, Y., Wang, T.T., Wang, B., Chang, W., Cao, J.L., Lu, M.X., and Zhang, L., *J. Renewable Mater.,* 2022, vol. 10, no. 2, p. 301. https://doi.org/10.32604/JRM.2021.015518
27. Liao, L.L., Mo, S., Luo, H.Q., and Li, N.B., *J. Colloid Interface Sci.,* 2018, vol. 520, p. 41. https://doi.org/10.1016/j.jcis.2018.02.071
28. Wu, Y.D., Guo, L., and She, Y.B., *J. Mol. Liq.,* 2020, vol. 346, p. 117858. https://doi.org/10.1016/j.molliq.2021.117858
29. Bacca, K.R.G., Lopes, N.F., Marcolino, J.B., Grasel, F.D.S., and Costa, E.M.D., *Mater. Corros.,* 2020, vol. 71, no. 1, p. 155. https://doi.org/10.1002/maco.201910963
30. Ikeuba, I., Ita, B.I., Okafor, P.C., Ugi, B.U., and Kporokpo, E.B., *Prot. Met. Phys. Chem. Surf.,* 2015, vol. 51, no. 6, p. 1043. https://doi.org/10.1134/S2070205115060118
31. Alibakhshi, E., Ramezanzadeh, M., Bahlakeh, G., Ramezanzadeh, B., Mahdavian, M., and Motamedi, M., *J. Mol. Liq.,* 2018, vol. 255, p. 185. https://doi.org/10.1016/j.molliq.2018.01.144
32. Bahlakeh, G., Ramezanzadeh, B., Dehghani, A., and Ramezanzadeh, M., *J. Mol. Liq.,* 2019, vol. 283, p. 174. https://doi.org/10.1016/j.molliq.2019.03.086
33. Tang, M., Li, X.H., Deng, S.D., and Lei, R., *J. Mol. Liq.,* 2021, vol. 344, p. 117926. https://doi.org/10.1016/j.molliq.2021.117926
34. Singh, A., Lin, Y.H., Ebenso, E.E., Liu, W.L., Pan, J., and Huang, B., *J. Ind. Eng. Chem.,* 2015, vol. 24, p. 219. https://doi.org/10.1016/j.jiec.2014.09.034
35. Dehghani, A., Bahlakeh, G., Ramezanzadeh, B., and Ramezanzadeh, M., *J. Mol. Liq.,* 2019, vol. 279, p. 603. https://doi.org/10.1016/j.molliq.2019.02.010
36. Amarowicz, R., Troszyńska, A., and Shahidi, F., *J. Food Lipids,* 2010, vol. 12, no. 4, p. 344. https://doi.org/10.1111/j.1745-4522.2005.00029.x
37. Fernandes, C.M., Fagundes, T.D.S.F., Santos, N.E.D., Rocha, T.S.D.M., Garrett, R., Borges, R.M., Muricy, G., Valverde, A.L., and Ponzio, E.A., *Electrochim. Acta,* 2019, vol. 312, p. 137. https://doi.org/10.1016/j.electacta.2019.04.148
38. Shekhar, C., Jaiswal, A., Ji, G., and Prakash, R., *Mater. Today: Proc.,* 2021, vol. 44, no. 1, p. 2267. https://doi.org/10.1016/j.matpr.2020.12.368
39. Mostafatabar, A.H., Dehghani, A., Ghahremani, P., Bahlakeh, G., and Ramezanzadeh, B., *J. Mol. Liq.,* 2022, vol. 346, p. 118344. https://doi.org/10.1016/j.molliq.2021.118344
40. Tehrani, M.E.H.N., Ghahremani, P., Ramezanzadeh, M., Bahlakeh, G., and Ramezanzadeh, B., *J. Environ. Chem. Eng.,* 2021, vol. 9, p. 105256. https://doi.org/10.1016/j.jece.2021.105256
41. Lebrini, M., Suedile, F., Salvin, P., Roos, C., Zarrouk, A., Jama, C., and Bentiss, F., *Surf. Interfaces,* 2020, vol. 20, p. 100588. https://doi.org/10.1016/j.surfin.2020.100588
42. Saraswat, V., Kumari, R., and Yadav, M., *J. Phys. Chem. Solids,* 2021, vol. 160, no. 25, p. 110341. https://doi.org/10.1016/j.jpcs.2021.110341
43. Azzouzi, M.E., Azzaoui, K., Warad, I., Hammouti, B., Shityakov, S., Sabbahi, R., Saoiabi, S., Youssoufi, M.H., Akartasse, N., and Jodeh, S., *J. Mol. Liq.,* 2022, vol. 347, p. 118354. https://doi.org/10.1016/j.molliq.2021.118354
44. Khamaysa, O.M.A., Selatnia, I., Lgaz, H., Sid, A., Lee, H.-S., Zeghache, H., Benahmed, M., Ali, I.H., and Mosset, P., *Colloids Surf., A,* 2021, vol. 626, p. 127047. https://doi.org/10.1016/J.COLSURFA.2021.127047
45. Sanaei, Z., Shahrabi, T., and Ramezanzadeh, B., *Dyes Pigm.,* 2017, vol. 139, p. 218. https://doi.org/10.1016/j.dyepig.2016.12.002
46. Hashim, N.Z.N., Anouar, E.H., Kassim, K., Zaki, H.M., Alharthi, A.I., and Embong, Z., *Appl. Surf. Sci.,* 2019, vol. 476, no. 5, p. 861. https://doi.org/10.1016/j.apsusc.2019.01.149

47. Chen, Z., Wang, M., Fadhil, A.A., Fu, C.Y., Chen, T.Q., Chen, M.J., Khadom, A.A., and Mahood, H.B., *Colloids Surf., A,* 2021, vol. 627, p. 127209. https://doi.org/10.1016/j.colsurfa.2021.127209

48. Bouanis, M., Tourabi, M., Nyassi, A., Zarrouk, A., Jama, C., and Bentiss, F., *Appl. Surf. Sci.,* 2016, vol. 389, no. 12, p. 952. https://doi.org/10.1016/j.apsusc.2016.07.115

49. Ismail, A.S. and Farag, A.A., *Surf. Interfaces,* 2020, vol. 19, p. 100483. https://doi.org/10.1016/j.surfin.2020.100483

50. Xu, C., Li, W.P., Tan, B.C., Zuo, X.L., and Zhang, S.T., *J. Mol. Liq.,* 2022, vol. 345, p. 116996. https://doi.org/10.1016/J.MOLLIQ.2021.116996

51. Bidi, M.A., Azadi, M., and Rassouli, M., *Mater. Today Commun.,* 2020, vol. 24, p. 100996. https://doi.org/10.1016/j.mtcomm.2020.100996

52. Rathod, M.R., Rajappa, S.K., Minagalavar, R.L., Praveen, B.M., Devendra, B.K., and Kittur, A.A., *Inorg. Chem. Commun.,* 2022, vol. 140, p. 109488. https://doi.org/10.1016/J.INOCHE.2022.109488

53. Hamdani, N.E., Fdil, R., Tourabi, M., Jama, C., and Bentiss, F., *Appl. Surf. Sci.,* 2015, p. 1294. https://doi.org/10.1016/j.apsusc.2015.09.159

54. Silva, M.V.L.D., Policarpi, E.D.B., and Spinelli, A., *J. Taiwan Inst. Chem. Eng.,* 2021, vol. 129, p. 342. https://doi.org/10.1016/J.JTICE.2021.09.026

55. Lin, B.L., Shao, J.J., Zhao, C., Zhou, X.X., He, F., and Xu, Y.Y., *J. Mol. Liq.,* 2023, vol. 375, p. 121296. https://doi.org/10.1016/j.molliq.2023.121296

56. Lin, B.L., Shao, J.J., Xu, Y.Y., Lai, Y.M., and Zhao, Z.N., *Arabian J. Chem.,* 2021, vol. 14, no. 5, p. 103114. https://doi.org/10.1016/j.arabjc.2021.103114

57. Zakeri, A., Bahmani, E., and Aghdam, A.S.R., *Corros. Commun.,* 2022, vol. 5, p. 25. https://doi.org/10.1016/j.corcom.2022.03.002

58. Thoume, A., Elmakssoudi, A., Left, D.B., Benzbiria, N., Benhiba, F., Dakir, M., Zahouily, M., Zarrouk, A., Azzi, M., and Zertoubi, M., *Chem. Data Collect.,* 2020, vol. 30, p. 100586. https://doi.org/10.1016/j.cdc.2020.100586

59. Tan, B., Xiang, B., Zhang, S., Qiang, Y., Xu, L., Chen, S., and He, J., *J. Colloid Interface Sci.,* 2021, vol. 582, part B, p. 918. https://doi.org/10.1016/j.jcis.2020.08.093

60. Tan, B.C., He, J.H., Zhang, S.T., Xu, C.L., Chen, S.J., Liu, H.Y., and Li, W.P., *J. Colloid Interface Sci.,* 2021, vol. 585, p. 287. https://doi.org/10.1016/j.jcis.2020.11.059

61. Asadi, N., Ramezanzadeh, M., Bahlakeh, G., and Ramezanzadeh, B., *J. Taiwan Inst. Chem. Eng.,* 2019, vol. 95, p. 252. https://doi.org/10.1016/j.jtice.2018.07.011

62. Zhang, X., Li, W.P., Yu, G.C., Zuo, X.L., Luo, W., Zhang, J., and Tan, B.C., *J. Mol. Liq.,* 2021, vol. 326, p. 115290. https://doi.org/10.1016/j.molliq.2021.115290

63. Wu, Y.X., Zhang, Y.M., Jiang, Y.M., Li, N., Zhang, Y.N., Wang, L., and Zhang, J.L., *Colloids Surf., A,* 2021, vol. 626, p. 126969. https://doi.org/10.1016/J.COLSURFA.2021.126969

64. Lima, K.C.D.S.D., Paiva, V.M., Perrone, D., Ripper, B., Simões, G., Rocco, M.L.M., Veiga, A.G.D., and D'Elia, E., *J. Mater. Res. Technol.,* 2020, vol. 9, no. 6, p. 12756. https://doi.org/10.1016/J.JMRT.2020.09.019

65. Sahraoui, M., Boulkroune, M., Chibani, A., Larbah, Y., and Abdessemed, A., *J. Bio-Tribo-Corros.,* 2022, vol. 8, no. 2, p. 1. https://doi.org/10.1007/S40735-022-00658-0

66. Popova, A., Christov, M., and Vasilev, A., *Corros. Sci.,* 2007, vol. 49, no. 8, p. 3290. https://doi.org/10.1016/j.corsci.2007.03.012

67. Eid, A.M., Shaaban, S., and Shalabi, K., *J. Mol. Liq.,* 2019, vol. 298, p. 111980. https://doi.org/10.1016/j.molliq.2019.111980

68. Hanini, K., Benahmed, M., Boudiba, S., Selatnia, I., Akkal, S., and Laouer, H., *Prot. Met. Phys. Chem. Surf.,* 2021, vol. 57, no. 1, p. 1. https://doi.org/10.1134/S2070205120060118

69. Elshami, A.A., Bonnet, S., Makhlouf, M.H., Khelidj, A., and Leklou, N., *Pigm. Resin Technol.,* 2020, vol. 49, no. 6, p. 501. https://doi.org/10.1108/PRT-09-2019-0078

70. Faydy, M.E., Lakhrissi, B., Jama, C., Zarrouk, A., Olasunkanmi, L.O., Ebenso, E.E., and Bentiss, F., *J. Mater. Res. Technol.,* 2020, vol. 9, no. 1, p. 727. https://doi.org/10.1016/j.jmrt.2019.11.014

71. Saxena, A., Prasad, D., Haldhar, R., Singh, G., and Kumar, A., *J. Mol. Liq.,* 2018, vol. 258, p. 89. https://doi.org/10.1016/j.molliq.2018.02.104

72. Kohn, W. and Sham, L.J., *Phys. Rev.*, 1965, vol. 137, no. 6A, p. 1697. https://doi.org/10.1103/PhysRev.137.A1697

73. Njoku, D.I., Ukaga, I., Ikenna, O.B., Oguzie, E.E., Oguzie, K.L., and Ibisi, N., *J. Mol. Liq.,* 2016, vol. 219, p. 417. https://doi.org/10.1016/j.molliq.2016.03.049

74. Khadom, A.A., Kadhim, M.M., Anaee, R.A., Mahood, H.B., Mahdi, M.S., and Salman, A.W., *J. Mol. Liq.,* 2021, vol. 343, p. 116978. https://doi.org/10.1016/J.MOLLIQ.2021.116978

75. Rani, A.T.J., Thomas, A., Arshad, M., and Joseph, A., *J. Mol. Liq.,* 2022, vol. 346, p. 117873. https://doi.org/10.1016/j.molliq.2021.117873

76. Aslam, R., Mobin, M., Huda, Obot, I.B., and Alamri, A.H., *J. Mol. Liq.,* 2020, vol. 318, p. 113982. https://doi.org/10.1016/j.molliq.2020.113982

77. Obot, I.B. and Gasem, Z.M., *Corros. Sci.,* 2014, vol. 83, p. 359. https://doi.org/10.1016/j.corsci.2014.03.008